

Determination of Shape and Sphericity of Silicon Quantum Dots Imaged by EFTEM-Tomography

Daniel Hiller,* Sebastian Gutsch, Julian López-Vidrier, Margit Zacharias, Sònia Estradé, Francesca Peiró, Irving Cruz-Matías, and Dolors Ayala

The shape of size-controlled silicon nanocrystals (Si NCs) embedded in SiO₂ is investigated by tomographic energy-filtered transmission electron microscopy (EFTEM). The sphericity of the quantum dots is determined by computational analyses. In contrast to other fabrication methods, we demonstrate that the NCs in superlattices are non-agglomerated, individual clusters with slightly oblate spheroidal shape. This allows for low surface-to-volume ratios and thereby low non-radiative defect densities as required by optoelectronic or sensing applications. A near-spherical shape is also a prerequisite for the direct comparison of Si quantum dots (QDs) with theoretical simulations.

1. Introduction

Silicon nanocrystals feature a tunable bandgap depending on their size and efficient luminescence in the visible and near-infrared spectrum. Applications of Si NCs are envisaged in various fields, for instance as optoelectronic material in Si-based light emitters,^[1,2] as sensor material with optical readout,^[3] or as


Dr. D. Hiller, Dr. S. Gutsch, Dr. J. López-Vidrier, Prof. M. Zacharias
Laboratory for Nanotechnology
Department of Microsystems Engineering (IMTEK)
University of Freiburg
Freiburg, Germany
E-mail: daniel.hiller@imtek.uni-freiburg.de

Dr. S. Estradé, Dr. F. Peiró
LENS-MIND Laboratory of Electron Nanoscopy
Electronics Department
University of Barcelona
Barcelona, Spain

Dr. S. Estradé, Dr. F. Peiró
Institute of Nanoscience and Nanotechnology In2UB
University of Barcelona
Barcelona, Spain

Dr. I. Cruz-Matías
Computer Science Department
University of Monterrey
Monterrey, Mexico

Dr. D. Ayala
Computer Science Department
Polytechnical University of Catalonia
Barcelona, Spain

 The ORCID identification number(s) for the author(s) of this article can be found under <https://doi.org/10.1002/pssc.201700216>.

DOI: 10.1002/pssc.201700216

label material in bio-imaging where its non-toxicity is a key factor.^[4] The average size of the Si quantum dots and the size distribution represent key factors for any application. Hence, the fabrication technique has to allow for both a controllable average NC size and a narrow size distribution. The SiO_x/SiO₂ superlattice approach^[5] meets these requirements.^[6,7]

Furthermore, an almost defect-free Si/SiO₂ interface quality can be achieved by H₂ passivation^[8] which in turn results in high luminescence quantum yields (QY) of ≈25% at room temperature.^[9] Very large luminescence quantum yields were also achieved for Si QDs from gas phase synthesis^[10] and a hydrogen silsesquioxane based synthesis.^[11,12] In all cases, a defect-free surface

passivation is pivotal. Since near-spherical entities have the smallest surface-to-volume ratios, best passivation qualities are anticipated for such NCs. In addition, most simulations, theories, and models describing Si NCs mathematically rely on a regular, near-spherical shape.^[13–16] In Ref. ^[17] theoretical studies showed clearly how even tiny size and symmetry fluctuations affect the coupling between quantum dots. It seems to be plausible that Gibbs free energy minimization during NC growth should result in near-spherical shapes, however, this fact cannot be simply taken for granted. In contrast, 3-dimensional TEM imaging demonstrated with impressive clarity how wrong the assumption of predominantly spherically-shaped Si NCs grown from a thick SiO_x thin film is^[18]: Complex surface morphologies with high surface-to-volume ratios and agglomerated NCs were found. Nano-Si network structures instead of individual Si clusters were also shown for Si-rich carbide samples using electron tomography.^[19]

Generally, conventional TEM projection imaging modes are limited in their informational value. The inevitable integration of image information along the thickness of a TEM specimen (i.e., the viewing direction) leads to unacceptable artefacts since the dimensions of the Si NCs (as small as 2 nm) are an order of magnitude smaller than the thickness of typical TEM specimens. Electron tomography on the other hand provides 3-dimensional structural information and hence a route to circumvent the averaging problem of conventional projection microscopy.^[20]

Here, we investigate by means of energy-filtered TEM (EFTEM) tomography and a detailed image analysis the size distribution and the sphericity of Si NCs grown by the superlattice approach.

2. Experimental Details

Size-controlled Si NCs embedded in SiO₂ matrix are grown on Si substrates by thermal evaporation of a superlattice (SL) comprised of 20 SiO₂/SiO_{x=1.2} bilayer stacks and a 10 nm thick capping oxide followed by an annealing step (quartz tube furnace, 1100 °C, 1 h, N₂ ambient). The sample has 3 nm thick Si-rich oxide (SRO) layers and 5 nm thick SiO₂ spacing layers. Photoluminescence (PL) was measured with a LN₂-cooled CCD attached to a single grating monochromator under excitation of a HeCd laser (3.8 eV). The spectra were corrected for the spectral response of the setup. Wedge-shaped TEM specimen were prepared using standard mechanical polishing techniques followed by a short low energy, low angle ion-milling cleaning step. EFTEM tomography was performed using a 200 kV FEI Tecnai™ F20-ST TEM equipped with a Gatan Tridiem 865ER imaging spectrometer. Tilt series from -68° to +76° at an increment of 4° were acquired by obtaining Si-plasmon loss images at 17 eV with a 3 eV wide energy window. The number of projections was intentionally limited to 36 (in contrast to typically used 2° step widths) to minimize the total electron irradiation dose below the threshold where SiO₂ becomes unstable and Si NCs are formed by the electron beam that were not present before.^[6] Due to the limited tilt range objects appear elongated along the z-direction in the tomographic reconstruction, that is, the beam direction in the 0° projection image. The elongation factor can be estimated from the tilt range^[21] and is ≈1.3 for the conditions specified above. To determine the shape of the NCs, the tomograms were corrected by this elongation factor.

The tomography data is a 32-bit gray scale dataset in RAW format of size 131 × 281 × 332 (x-y-z; see abstract figure for the attribution of the axes). Several pre-processing steps have been applied. The original dataset has been converted to an 8-bit voxel model. Then it has been scaled via trilinear interpolation, to twice its size in order to better define the NCs shapes. After applying the mentioned elongation factor, the model has been cropped by removing the base plate. Finally, we have applied a binary threshold filter and removed noise with morphological opening and closing. For the threshold filter a gray value of 50 was selected, which yields the best segmentation of the corresponding connected components (CC). Further details can be found in Ref. ^[22]. The voxel size in the dataset is 0.17 nm (a dimension which is in accordance with the microscope resolution) and we considered only those CC with a volume >200 voxels, which gives a total of 731 CC. In order to compute the length measurements of each NC we have applied principal component analysis (PCA) to the voxel model.

3. Results and Discussion

The PL spectrum of the Si NC sample is shown in **Figure 1**. The PL peak can be fitted very well as a symmetrical Gaussian peak with a peak position of 808 nm. The full-width at half-maximum (FWHM) is 160 nm, which corresponds to ≈300 meV. Please note that a significant fraction of this peak width originates from the indirect optical transitions (phonon contribution), as shown by single QD spectroscopy in Ref. ^[23]. The other factor that increases the PL peak width is the NC-size distribution. The circumstance that the PL peak is symmetrical indicates already a

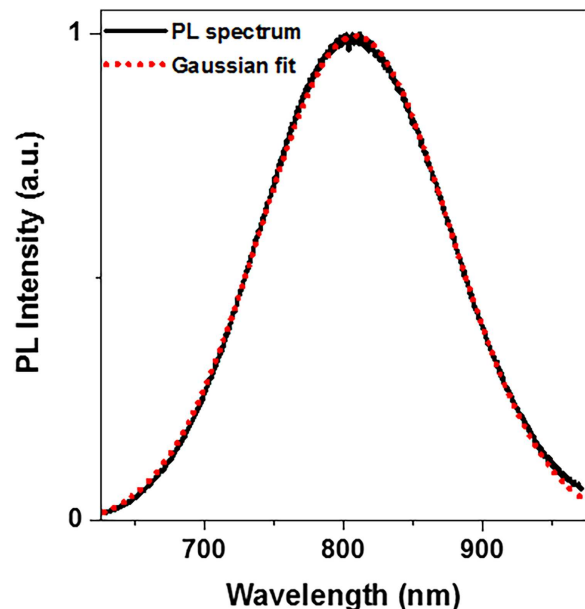


Figure 1. Photoluminescence spectrum of the Si NC sample with 3 nm thick SRO layers (black line) and a Gaussian fit (red dotted line).

quite regular size distribution. As we will show below this is indeed observed by EFTEM-tomography, which implicates that the reverse conclusion can be generalized to this sample system: If the PL peak is highly symmetrical and Gaussian-like, the luminescence originates from a Si NC-ensemble with an at least close-to-Gaussian size distribution.

Figure 2(a) shows a conventional EFTEM projection image in cross-section geometry. The layered arrangement of the Si NC superlattice is clearly seen. For comparison, a side view of the volume renderings of the tomographic reconstructions is shown in **Figure 2(b)**. In contrast to **Figure 2(a)** it is more difficult to observe individual NCs in **Figure 2(b)** since it was taken at a thicker part of the specimen. Due to overlap, individual NCs can hardly be distinguished in the side view of the 3D reconstruction when the interface planes are aligned parallel to the viewing direction. To circumvent this problem, **Figure 2(c)** shows a tilted view of only every second NC layer of the SL.

Please see the Supporting Information for a video of the 3D tomographic reconstruction. On first sight it is obvious that the Si NCs in the SL have a near-spherical shape and that they are well-separated from each other, that is, no extended Si agglomerates are found.

The tomographic EFTEM raw data was converted into a voxel model and the connected components (CCs), which represent the Si NCs, are analyzed in terms of their size and shape. Please note that voxels of <1 nm³ are considered as artefacts and are excluded from the analysis, since such ultra-small crystalline Si features do not exist.^[24] Since each voxel is of slightly irregular shape we first consider the sphere-equivalent diameter d_{sphere} , that is, the whole voxel volume is considered to be a sphere. **Figure 3** shows that these NC-diameters (dark gray bars) can be fitted with a quite sharp log-normal distribution (thick dashed line), as proposed before for size-controlled Si NCs.^[6,7] The log-normal fit does not deviate significantly from a Gaussian fit (thin

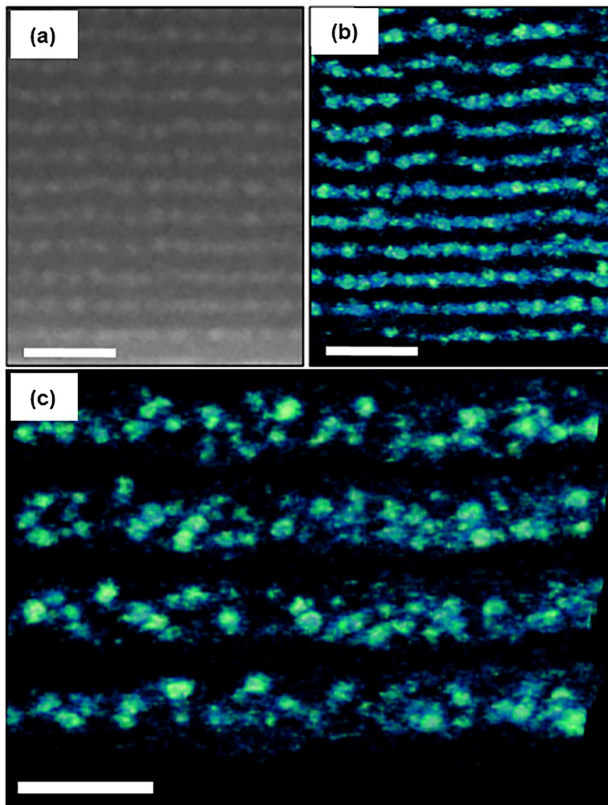


Figure 2. a) EFTEM projection image taken from a thinner part of the specimen. b) EFTEM tomographic reconstructions taken from a thicker part of the specimen. c) Tilted reconstruction with respect to the interface planes, so that the in-plane arrangement of the Si NCs is visible; for clarity, only every second NC layer of the SL is displayed. All scale bars correspond to 20 nm.

solid line), so that the size distribution can be considered as quite symmetric, as suggested by PL.

The mean size of this distribution is only ≈ 1.9 nm although the initial SRO thickness was 3 nm. This difference is significantly larger than typically observed for the NC formation in 2-dimensionally confined SRO layers of only few nanometers thickness [6,7,25]. Interestingly, the mean diameter of the NC-extent in all three dimensions, that is, $d_{\text{mean}} = (a + b + c)/3$, exhibits a mean size of ≈ 2.6 nm as shown by the light gray bars in Figure 3. The d_{mean} -distribution can be fitted by log-normal and Gaussian functions with equal quality. The mean diameter is much closer to the expected NC-size according to the initial SRO thickness. Apparently, the approximation of purely spherical CCs is not fully correct, otherwise d_{mean} and d_{sphere} would have the same value.

In order to quantify the deviation from the perfect spherical shape the sphericity of the NCs is computed. We calculated the so-called true sphericity index Ψ as defined in Ref. [26]:

$$\Psi = \frac{S_n}{S} = \frac{\sqrt[3]{36\pi V^2}}{S}$$

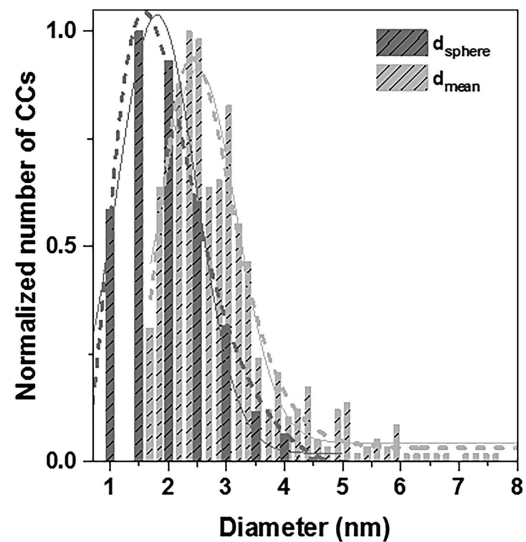


Figure 3. Diameter distribution of the connected components in the voxel model of the tomographic EFTEM reconstruction analysed as sphere-equivalent volume diameter and as average diameter via $d_{\text{mean}} = (a + b + c)/3$. Both NC size distributions are well described by a log-normal fit (dashed lines). Gaussian fits (thin solid lines) deviate not much but describe the distributions slightly less accurately especially in the case of d_{sphere} .

where V and S are the volume and surface area of the object respectively, and S_n the nominal surface area. The volume V is derived directly from the voxel model. The surface S is computed from the voxel model using a method that calculates an accurate approximation of the underlying surface.[27] The values of the true sphericity are plotted in Figure 4(a). There are almost no perfectly spherical NCs with $\Psi = 1.0$, but only few NCs have significantly small Ψ -values. The distribution can be well fitted by a logit-normal distribution (also known as logistic normal distribution) with a peak value of $\Psi = 0.86$.

From the bare sphericity data we cannot derive if the non-spherical shape is arbitrarily distributed over the three dimensions or whether it has a certain preferential direction. Therefore, we plot in Figure 4(b) the in-plane diameter-ratio a/b (light gray bars). This ratio has a mean value of almost one and is well fitted by a Gaussian distribution (dotted line).

Hence, the lateral CC-sizes in the two planar dimensions of each SL-layer are equal, which is expected from the unrestricted self-organized NC-growth. In contrast, the diameter-ratio c/b (dark gray bars) has a mean value of only ≈ 0.6 . This implicates that the CC-size vertical to the SL-stacking direction is smaller than the planar size, which is supposed to be a consequence of the growth-confinement in this dimension by the SiO_2 barrier layers. Please note that the ratio c/a (not shown here for the sake of clarity) has similar values as c/b .

The resulting shape of Si NCs can be now described as oblate spheroids with a geometric flattening in the vertical z -dimension. Considering only the mean c/b ratio of ≈ 0.6 the relative eccentricity $e_{\text{rel}} = \sqrt{1 - \frac{c^2}{b^2}}$ with $b \approx a \approx 1$ can be estimated to $e_{\text{rel}} = 0.8$. This may appear to be a significant deviation from a truly spherical shape. However, the surface area of an oblate spheroid with that geometry has just $\approx 12\%$ more

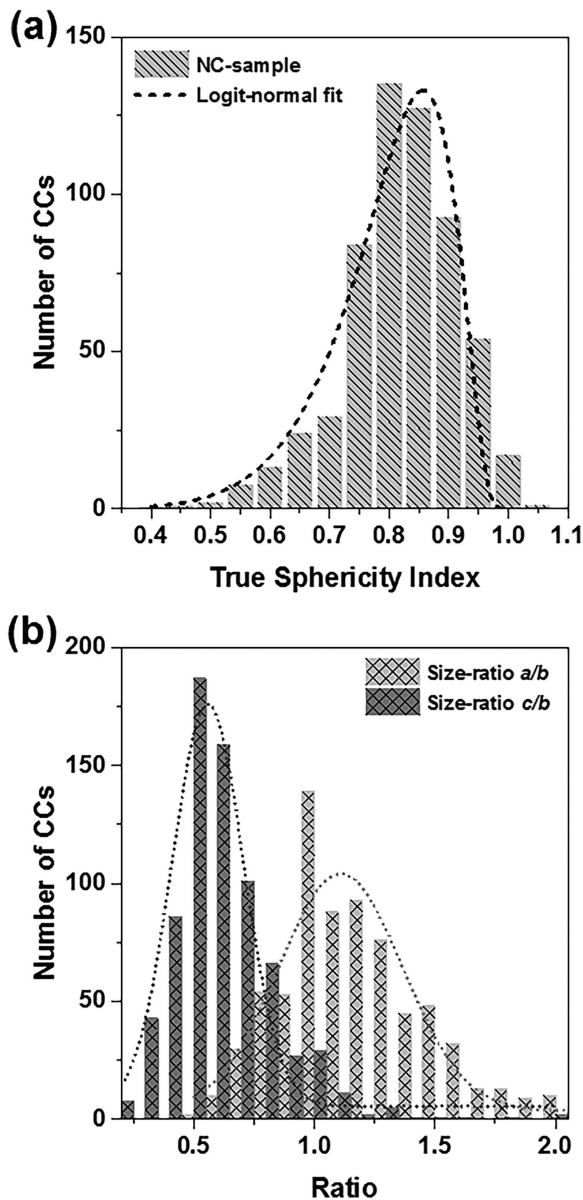


Figure 4. a) True sphericity index Ψ of the Si NC ensemble with a logit-normal fit (black dashed line). b) Ratios of the two lateral CC-sizes a and b (light gray bars) compared to the ratio of the vertical size c with the lateral size b . Both are well fitted by Gaussian distributions (dotted lines). While the mean lateral sizes are almost equal, the mean vertical size is significantly smaller.

surface-to-volume ratio than a real sphere. In spite of the relatively large eccentricity, this does not represent a large deviation of actual NCs with respect to what is ideally expected in terms of shape. Hence, the Si/SiO₂ interface defect density is not dramatically increased. Furthermore, the confinement of the exciton wavefunction is not significantly different from that in a real sphere and by far not as complex as in highly non-spherical (e.g., “horseshoe”-shaped) Si NCs.^[28,29] Finally, it should be investigated if that shape is universal for Si NCs in superlattices

or if this is unique to the fabrication via reactive thermal evaporation.

4. Conclusions

In conclusion, we demonstrated by means of EFTEM tomography that Si NCs embedded in a SiO₂ SL structure are of near-spherical shape. In contrast to NCs formed by annealing thick SRO films, the SL assembly allows not only for a narrow size distribution but also ensures the absence of significant NC agglomeration. The voxel analysis of the EFTEM reconstruction results in a mean NC-size of 2.6 nm (in accordance with the 3 nm initial SRO thickness) and a peak true sphericity index Ψ of 0.86, which indicates a deviation from a perfectly spherical NC shape. Whereas the two mean NC-diameters in the in-plane direction of the SL are equal, the vertical extend of the NCs is smaller. This constitutes a slightly oblate-spheroidal shape of the Si NCs.

Supporting Information

Supporting Information is available from the Wiley Online Library or from the author.

Acknowledgements

We gratefully acknowledge Lena F. Kourkoutis (Cornell University) for EFTEM-tomography. This work was partially supported by the national Projects TIN2008-02903 and TIN2011-24220 of the Spanish government. We also acknowledge the financial support from the Spanish Ministry of Economy, Industry and Competitiveness through the project MAT2016-79455-P, with support of FEDER funds.

Conflict of Interest

The authors declare no conflict of interest.

Keywords

energy-filtered transmission electron tomography, silicon nanocrystals, silicon quantum dots, sphericity

Received: August 1, 2017

Published online:

- [1] R. J. Anthony, K.-Y. Cheng, Z. C. Holman, R. J. Holmes, U. R. Kortshagen, *Nano Lett.* **2012**, *12*, 2822.
- [2] F. Maier-Flaig, J. Rinck, M. Stephan, T. Bocksrocker, M. Bruns, C. Kübel, A. K. Powell, G. A. Ozin, U. Lemmer, *Nano Lett.* **2013**, *13*, 475.
- [3] A. Nguyen, C. M. Gonzalez, R. Sinelnikov, W. Newman, S. Sun, R. Lockwood, J. G. C. Veinot, A. Meldrum, *Nanotechnology* **2016**, *27*, 105501.
- [4] B. F. P. McVey, R. D. Tilley, *Acc. Chem. Res.* **2014**, *47*, 3045.
- [5] M. Zacharias, J. Heitmann, R. Scholz, U. Kahler, M. Schmidt, J. Bläsing, *Appl. Phys. Lett.* **2002**, *80*, 661.

- [6] S. Gutsch, D. Hiller, J. Laube, M. Zacharias, C. Kübel, *Beilstein J. Nanotechnol.* **2015**, 6, 964.
- [7] J. Laube, S. Gutsch, D. Wang, C. Kübel, M. Zacharias, D. Hiller, *Appl. Phys. Lett.* **2016**, 108, 043106.
- [8] M. Jivanescu, D. Hiller, M. Zacharias, A. Stesmans, *Euro Phys. Lett.* **2011**, 96, 27003.
- [9] J. Valenta, M. Greben, S. Gutsch, D. Hiller, M. Zacharias, *Appl. Phys. Lett.* **2014**, 105, 243107.
- [10] L. Mangolini, D. Jurbergs, E. Rogojina, U. Kortshagen, *J. Lumin.* **2006**, 121, 327.
- [11] C. M. Hessel, E. J. Henderson, J. G. C. Veinot, *Chem. Mater.* **2006**, 18, 6139.
- [12] F. Sangghaleh, I. Sychugov, Z. Yang, J. G. C. Veinot, J. Linnros, *ACS Nano* **2015**, 9, 7097.
- [13] D. König, J. Rudd, M. A. Green, G. Conibeer, *Phys. Rev. B* **2008**, 78, 035339.
- [14] C. Bulutay, *Phys. Rev. B* **2007**, 76, 205321.
- [15] D. König, D. Hiller, S. Gutsch, M. Zacharias, *Adv. Mat. Int.* **2014**, 1, 1400359.
- [16] D. König, *AIP Adv.* **2016**, 6, 085306.
- [17] J. W. Luo, P. Stradins, A. Zunger, *Energy Environ. Sci.* **2011**, 4, 2546.
- [18] A. Yurtsever, M. Weyland, D. A. Muller, *Appl. Phys. Lett.* **2006**, 89, 151920.
- [19] L. Xie, K. Jarolimek, V. Kocovski, J. Rusz, M. Zeman, R. A. C. M. M. van Swaaij, K. Leifer, *Nanoscale* **2017**, 9, 6703.
- [20] J. Frank, *Electron Tomography: Three-Dimensional Imaging With the Transmission Electron Microscope*, Plenum, New York **1992**.
- [21] M. Radermacher, W. Hoppe, *Proceedings of the 7th European Congress on Electron Microscopy* **1980**, 1, 132.
- [22] I. Cruz-Matías, D. Ayala, D. Hiller, S. Gutsch, M. Zacharias, F. Peiró, *Sphericity and Roundness Computation for Particles using the Extreme Vertices Model*, Graphical Models, (under review).
- [23] J. Valenta, R. Juhasz, J. Linnros, *Appl. Phys. Lett.* **2002**, 80, 1070.
- [24] M. Zacharias, P. Streitenberger, *Phys. Rev. B* **2000**, 62, 8391.
- [25] A. M. Hartel, D. Hiller, S. Gutsch, P. Löper, S. Estradé, F. Peiró, B. Garrido, M. Zacharias, *Thin Solid Films* **2011**, 520, 121.
- [26] H. Wadell, *J. Geol.* **1932**, 40, 443.
- [27] G. Windreich, N. Kiryati, G. Lohmann, *Pattern Recognition* **2003**, 36, 2531.
- [28] L. F. Kourkoutis, X. Hao, S. Huang, B. Puthen-Veettil, G. Conibeer, M. A. Green, I. Perez-Wurfl, *Nanoscale* **2013**, 5, 7499.
- [29] B. Puthen Veettil, D. König, S. Huang, R. Patterson, G. Conibeer, *J. Appl. Phys.* **2017**, 121, 054306.